Numerical analysis of long-range surface plasmon polariton modes in nanoscale plasmonic waveguides

Alexey V. Krasavin* and Anatoly V. Zayats

Centre for Nanostructured Media, International Research Centre for Experimental Physics, The Queen's University of Belfast, Belfast, BT7 1NN, UK

**Corresponding author: a.krasavin@qub.ac.uk*

Received March 12, 2010; revised May 27, 2010; accepted June 1, 2010; posted June 3, 2010 (Doc. ID 125450); published June 15, 2010

Guiding properties of nanoscale metallic wire waveguides embedded in a semiconductor are discussed. By performing eigenmode numerical simulations of the waveguide and continually varying the geometrical cross-section parameters, we have obtained comprehensive mode characteristics, such as the effective refractive index, effective mode area, and propagation length, that provide full guided mode description. This allows us to gain insight into possible waveguide applications using the figures of merit. Amplification and polarization manipulation of a plasmonic signal in such a waveguide have also been considered.

OCIS codes: 130.0130, 250.5403.

Surface plasmon polariton (SPP) waves are attracting increasing attention as promising information carriers in highly integrated optical devices due to their ability to localize electromagnetic fields on a subwavelength scale. Surface plasmon polaritons are electromagnetic excitations coupled to electron oscillations propagating in a wavelike fashion along a metal–dielectric interface [1,2]. Being surface waves, they naturally localize a photonic signal in one dimension, making it possible to overcome the diffraction limit of three-dimensional optics. Moreover, SPP waveguides can be incorporated into existing information-processing circuits, presenting the possibility of creating hybrid electronic/photonic devices.

Several approaches for SPP waveguides have been proposed, such as guiding in the gap between two metallic walls [3], along a row of metallic nanoparticles [4,5], along a channel [6] or a wedge [7] on the surface of a metallic film, and as a metallic wire embedded in a dielectric [8]. The latter waveguide provides the longest SPP propagation length due to its ability to support the long-range SPP mode. When the metallic film becomes thin enough (of the order of several tens of nanometers), the SPP modes on both surfaces of the film become coupled. This results in lifting the degeneration; two propagating SPP modes appear with symmetric and asymmetric field distributions [8]. The mode with the symmetric distribution has a very small amount of the field localized in the metal, providing propagation lengths in the millimeter range.

Despite great attention being given to metallic stripe SPP waveguides, both theoretical and experimental [8–14], there is a gap in understanding how the long-range mode behaves in waveguides having truly nanoscale dimensions. This is the key point studied in this Letter. Moreover, we present continuous mapping of the mode parameters as a function of waveguide cross section, covering all possible nanoscale waveguide widths and heights. This knowledge is extremely important for the optimization of the waveguide for different plasmonic applications. We apply rigorous finite element method eigenmode simulations of the waveguide (COMSOL Multiphysics software), additionally taking advantage of the mode symmetries. This allows us to perform a complete analysis of the mode characteristics in subwavelength metallic stripe SPP waveguides. The mode is fully characterized in terms of effective refractive index, field localization properties, and propagation length in a complete range of subwavelength cross sections. The results are also used to calculate the figures of merit.

We studied a gold (n_1) waveguide of a rectangular cross section embedded in high refractive index InGaAsP-based material (n_2) (Fig. 1 inset). The choice of a noble metal ensures a long propagation distance, while an appropriate choice of dielectric enables introduction of gain, making the propagation lossless or even achieving SPP amplification [13]. We set the design wavelength $\lambda = 1550$ nm to demonstrate the potential applications of these plasmonic waveguides in telecommunications. The refractive indices for the materials $n_1 = 0.55 - 11.5i$ and $n_2 = 3.3737$ were taken from [15] and [13], respectively. A careful investigation of mode structure of a metallic stripe waveguide shows that it supports several modes, corresponding to different field symmetries [8,14]. Here we concentrate on the mode with the electromagnetic field directed

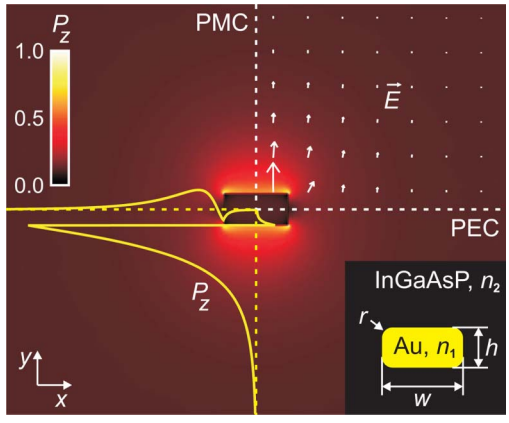

Fig. 1. (Color online) Field map of power flow P_z of the long-range SPP mode supported by a 200 nm × 100 nm waveguide at $\lambda = 1550$ nm. Solid curves correspond to the vertical and horizontal cross sections of the power flow P_z. Arrows show the direction of the electric field. Inset: studied Au($n_1 = 0.55–11.5i$)/InGaAsP($n_2 = 3.3737$) metallic wire waveguide with width w and height h, having corners rounded with $r = 5$ nm.

predominately in the vertical direction and having a symmetric field distribution (Fig. 1). This mode, in the limit of a thin waveguide, corresponds to the long-range SPP mode, having the longest propagation distance. In the eigenmode simulations, the waveguide was sliced along the horizontal and vertical symmetry axes. A perfect electric conductor boundary condition (PEC, $\mathbf{n} \times \mathbf{E} = 0$) was set on the horizontal boundary, a perfect magnetic boundary condition (PMC, $\mathbf{n} \times \mathbf{H} = 0$) on the vertical boundary, and only the top-right quarter of the domain was simulated. This allows us to discriminate the mode with the required field symmetry and also to reduce the numerical complexity of the model.

A complete set of mode characteristics were investigated as a function of the waveguide width w and height h (see the inset to Fig. 1). The corners of the waveguide were rounded with a radius of $r = 5$ nm to avoid field singularities and also because the fabrication of sharp corners is rather difficult. All three main mode characteristics, the effective refractive index $\mathrm{Re}(n_{\mathrm{eff}})$ ($n_{\mathrm{eff}} = k_{\mathrm{SPP}}^{\mathrm{mode}}/k$, where $k = 2\pi/\lambda$ is a free space wave vector), the effective mode area S, and propagation length are closely connected and generally define the trade-off between mode localization and propagation (Fig. 2). The effective area was defined as an area inside the constant magnitude contour, encircling (1–$3e^{-2}$) part (around 60%) of the total intensity integral in the dielectric, plus the area of the metal section supporting it (see the inset). This corresponds to the part of the intensity encircled by a $1/e$ field decay contour in the case of the Gaussian mode distribution. Here we used an integral, opposed to a magnitude (as in [12]) condition for the level defining the contour, because, with various waveguide cross sections, various mode profiles should be expected. The propagation length $L_{\mathrm{prop}} = \lambda/(4\pi \mathrm{Im}(n_{\mathrm{eff}}))$ is defined as a distance at which the energy of the mode decreases in e times.

At the smallest waveguide cross section studied, 50×50 nm, the fields are pushed out of the metal due to the symmetric field configuration of the mode. This leads to the largest effective mode area (the fields extend on a distance $\sim$10 μm) and the effective refractive index of the mode ($\mathrm{Re}(n_{\mathrm{eff}}) = 3.3738$) is, therefore, close to the refractive index of the surrounding dielectric material ($n_2 = 3.3737$). The mode in this case is very weakly localized. At the same time, a smaller amount of field in the metal leads to smaller Ohmic losses, resulting in an increase of the propagation length up to 6 mm. At the other end of the geometric parameters range ($h = 450$ nm), we observe that the effective refractive index of the mode increases, approaching $\mathrm{Re}(n_{\mathrm{eff}}) = 3.7$–$4$. Now the mode becomes localized at distances of less than 100 nm next to the metal and the propagation length decreases dramatically down to several micrometers. This propagation length is even smaller than that for an SPP wave on a semi-infinite InGaAsP/Au interface ($L_{\mathrm{prop}}^{s\text{-inf}} = 7.8$ μm). This is because, at these waveguide sizes, the corners of the waveguide become well separated from each other, so the mode decomposes into a set of corner SPP modes [14], having very short propagation distances.

Another interesting region is thin waveguides, having h of the order of 50 nm. As we make the thin metallic stripe wider, the general trend is the decrease of the propagation length and the mode area. However, the propagation distances continue to be quite large, being more than 25 μm for the widest stripes studied. The propagation distance approaches that of a mode supported by an infinite metallic film asymptotically with $L_{\mathrm{prop}}^{\mathrm{film}} = 17.2$ μm. Overall, depending on the waveguide cross section, the symmetric SPP modes in nanoscale metallic waveguides cover the whole range of propagation characteristics, starting from those close to conventional dielectric waveguides (several-micrometer mode size, millimeter-range propagation distance), becoming similar to dielectric-loaded or channel SPP waveguides (fraction of micrometer mode size, several tens of micrometers propagation distance) and finally transforming into highly localized corner modes [14].

The symmetry of the long-range mode field distribution allows feasible end-fire mode launching using a standard optical fiber. Since a signal in telecommunication fiber lines is generally unpolarized, metallic waveguides with a square cross section are beneficial. Both polarization components will equally couple to the waveguide and propagate along it with the same effective index and propagation length. On the other hand, for some functions, it is desirable to discriminate one polarization with respect to the other. In this case, asymmetric, wide, and thin, waveguides should be used. The component with the electric field perpendicular to the long edge of the waveguide has a propagation length much larger than the one having the electric field perpendicular to the short edge [Fig. 2(c)].

To compare waveguides with different cross sections and find a compromise between the localization of the mode and its propagation length, figures of merit M_1, M_2, and M_3 (as defined in [12]) have been calculated. The first figure of merit, $M_1 = 2\sqrt{\pi} L_{\mathrm{prop}}/\sqrt{S}$, is a straightforward ratio between the mode propagation length and its size [Fig. 3(a)]. In the plot mapping M_1 for various

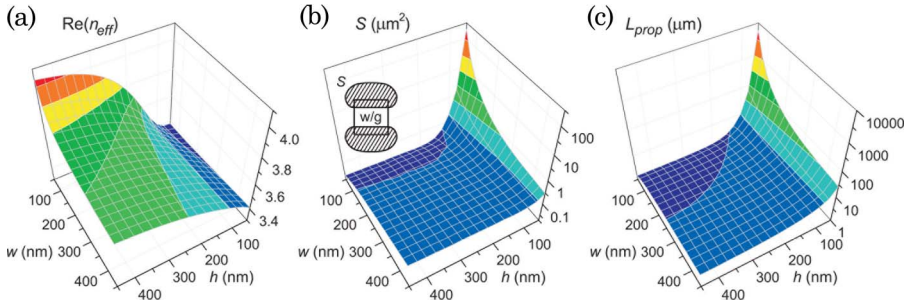

Fig. 2. (Color online) (a) Real part of the effective refractive index, (b) effective mode area, and (c) propagation length of the mode as functions of waveguide geometrical parameters for Au nanowire waveguide embedded in InGaAsP.

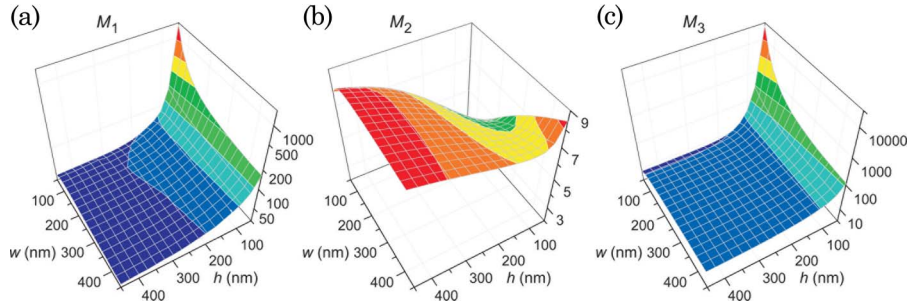

Fig. 3. (Color online) Figures of merit: (a) $M_1 = 2\sqrt{\pi}L_{\text{prop}}/\sqrt{S}$, (b) $M_2 = (\text{Re}(n_{\text{eff}}) - n_2)/\text{Im}(n_{\text{eff}})$, and (c) $M_3 = \text{Re}(n_{\text{eff}})/(2\pi\text{Im}(n_{\text{eff}}))$ as functions of waveguide geometrical parameters for Au nanowire waveguide embedded in InGaAsP.

cross sections, there is a clear maximum at the smallest waveguide sizes, indicating that, seemingly, these waveguides would be the most beneficial. However, they also correspond to the case of the smallest effective refractive index and the largest mode size, leading to poor field confinement. Another characteristic of the modes is expressed in M_2 [Fig. 3(b)], which defines the difference in the effective refractive index of the mode and the refractive index of the surrounding dielectric $M_2 = (\text{Re}(n_{\text{eff}}) - n_2)/\text{Im}(n_{\text{eff}})$. For higher values of M_2, it is possible to bend the waveguides with smaller radii before the mode at the outer side of the bend becomes coupled to light. The last figure of merit, $M_3 = \text{Re}(n_{\text{eff}})/(2\pi\text{Im}(n_{\text{eff}}))$ [Fig. 3(c)] represents a straightforward measure of waveguide applicability for microresonators or nanoresonators. Because of their largest propagation length, the waveguides with the smallest cross sections appear to be the most beneficial for these applications. Finally, because the refractive index of silicon at $\lambda = 1550$ nm ($n_{\text{Si}} = 3.48$) is close to that of InGaAsP, similar mode characteristics should be expected for waveguides embedded in silicon. Moreover, the plasmonic properties of aluminum at this wavelength are similar to that for gold ($n_{\text{Al}} = 1.44 - 16i$ [15]; for example, for a $200(w)$ nm $\times$ $50(h)$ nm waveguide considered here, $n_{\text{eff}}^{\text{Au}} = 3.382 - 0.00158i$, $S^{\text{Au}} = 1.15\ \mu\text{m}^2$, $n_{\text{eff}}^{\text{Al}} = 3.375 - 0.00085i$, and $S^{\text{Al}} = 5.49\ \mu\text{m}^2$, leading to $M_1^{\text{Al}}/M_1^{\text{Au}} = 0.85$). Therefore Si/Al waveguides, showing guiding properties similar to those of the waveguides considered here, will additionally be compatible with the existing CMOS fabrication processes.

A very essential hurdle to overcome in implementing SPP waves as photonic signal carriers is compensation of Ohmic losses, responsible for their finite propagation length. It is possible to do so using an active medium as a dielectric component of the waveguide [13]. Simulations show that the gain in the dielectric medium surrounding the waveguide, required for lossless SPP mode propagation (with $\text{Im}(n_{\text{eff}}) = 0$), is $\text{Im}(\epsilon_2) = 0.0117$ for a 200 nm $\times$ 100 nm waveguide and only $\text{Im}(\epsilon_2) = 0.00153$ for a 200 nm $\times$ 50 nm waveguide. These correspond to gain coefficients of 949 and 124 cm^{-1}, respectively. These values can be achieved with InGaAsP-based active medium for which we performed our simulations [16].

In conclusion, we present an exhaustive numerical investigation of the guiding performance of nanoscale metallic stripe SPP waveguides for the case of long-range SPP modes. We provide full mode characterization in terms of the effective refractive index, effective area, and propagation length for the whole range of subwavelength metallic wire cross sections. We have also described polarization management in such waveguides through the choice of the appropriate width/height ratio and demonstrated a realistic approach to lossless mode propagation. This comprehensive study should enable an informed choice to be made with respect to the geometrical parameters of the waveguide depending on the particular application.

This work was supported in part by the Engineering and Physical Sciences Research Council (EPSRC) (UK) and the European Commission's Framework Programme 6 Project PLASMOCOM.

References

1. H. Raether, *Surface Plasmons on Smooth and Rough Surfaces and Gratings* (Springer-Verlag, 1988).
2. A. V. Zayats, I. I. Smolyaninov, and A. A. Maradudin, Phys. Rep. **408**, 131 (2005).
3. L. Liu, Z. Han, and S. He, Opt. Express **13**, 6645 (2005).
4. S. A. Maier, M. L. Brongersma, P. G. Kik, S. Meltzer, A. A. G. Requicha, and H. A. Atwater, Adv. Mater. **13**, 1501 (2001).
5. G. A. Wurtz, W. Dickson, D. O'Connor, R. Atkinson, W. Hendren, P. Evans, R. Pollard, and A. V. Zayats, Opt. Express **16**, 7460 (2008).
6. S. I. Bozhevolnyi, V. S. Volkov, E. Devaux, J.-Y. Laluet, and T. W. Ebbesen, Nature **440**, 508 (2006).
7. A. Boltasseva, V. S. Volkov, R. B. Nielsen, E. Moreno, S. G. Rodrigo, and S. I. Bozhevolnyi, Opt. Express **16**, 5252 (2008).
8. P. Berini, Opt. Lett. **24**, 1011 (1999).
9. J.-C. Weeber, M. U. Gonzalez, A.-L. Baudrion, and A. Dereux, Appl. Phys. Lett. **87**, 221101 (2005).
10. P. Berini, Phys. Rev. B **61**, 10484 (2000).
11. A. Boltasseva, T. Nikolajsen, K. Leosson, K. Kjaer, M. S. Larsen, and S. I. Bozhevolnyi, J. Lightwave Technol. **23**, 413 (2005).
12. R. Buckley and P. Berini, Opt. Express **15**, 12174 (2007).
13. M. P. Nezhad, K. Tetz, and Y. Feinman, Opt. Express **12**, 4072 (2004).
14. J. Jung, T. Sondergaard, and S. I. Bozhevolnyi, Phys. Rev. B **76**, 035434 (2007).
15. E. D. Palik, ed., *Handbook of Optical Constants of Solids* (Academic, 1984).
16. T. Saitoh and T. Mukai, IEEE J. Quantum Electron. **23**, 1010 (1987).